TiO_2/ZnO/CuO/HDTMA-Br Composite for Photodegradation of Oxidative Compounds of Used Cooking Oil (UCO): Photodegradation of Free Fatty Acids and Peroxides

Adinda Pitaloka, Komar Sutriah*, Sri Mulijani, Mohammad Khotib

Department of Chemistry, IPB University, Bogor 16680, Indonesia

** Corresponding Author. E-mail: komar.sutriah@yahoo.com*
Telp: +62-812-9648-643, Fax: +62-812-9648-643

Abstract

Used cooking oil (UCO) contains peroxide and FFA, which can impede UCO processing and lower the quality of downstream products. The majority of pretreatment techniques currently in use have drawbacks, such as excessive chemical use. An alternative that is more successful and efficient is photocatalysis. No research has been conducted on the photodegradation of UCO using TiO_2/ZnO/CuO/HDTMA-Br composites. Precipitation was used to create the composite. The TiO_2/ZnO/CuO composite has a high crystallinity, specifically 74.54% in the 1 CMC-modified catalyst, according to the characterization results. The spectrum of the synthesized TiO_2/ZnO/CuO composite showed the presence of H_2O and CO_2 groups in addition to the primary groups of TiO_2, ZnO, and CuO. Additionally, the 1 CMC modification increased pore volume and surface area. The surfactant-modified composite exhibited a more consistent morphology, as observed by SEM analysis. The best results from photocatalytic testing at different temperatures, times, and surfactant concentrations were obtained at 120 °C for an hour with a surfactant concentration of 1 CMC. These results show that degradation using TiO_2/ZnO/CuO photocatalysts can lower the FFA and peroxide contents of UCO by 65% and 59%, respectively, under ideal conditions. This study focuses on FFA and peroxide value parameters as a preliminary investigation into alternative UCO pretreatment solutions.

Keywords: HDTMA-Br; Oxidative Compounds; Photodegradation; TiO_2/ZnO/CuO; Used Cooking Oil

1. Introduction

World oil consumption increased by 55 million metric tons (23.5%) from 2013 to 2023, according to the United States Department of Agriculture Data [1]. Given this level of consumption, there is bound to be an equally high level of production of used cooking oil (UCO). Environmental challenges associated with the disposal of used cooking oil include clogged drains, increased pollutant concentrations in lakes, and general ecological deterioration [2]. If ingested, used cooking oil also poses the danger of oxidative stress, which can cause cardiovascular disease, cancer, and neurodegenerative disorders [3]. Advancements in the production of biodiesel [4], biolubricants [5], biosurfactants [6], and biopolymer materials such as polyurethane [7] have made the reuse of UCO a critical, innovative solution to challenges in a circular economy. Considerable effort must be made to identify the best technological processes to optimise UCO degradation to a minimum and maximise the production of the economically valuable end product.

The quality of used cooking oil can be assessed by examining the percentage of free fatty acids (FFA) and peroxide value [8]. High FFA levels cause saponification during basic transesterification, thereby reducing product yield and complicating phase separation [9]. On the other hand, high PV and secondary oxidation products accelerate thermal and oxidative degradation, leading to undesirable odours and

colours and reducing the stability of downstream products [10]. Therefore, controlling FFA and PV at the upstream stage (pretreatment) is very important to improve the technical and economic effectiveness of UCO utilisation. Standard pretreatment methods reported in the literature include adsorption, chemical bleaching, and solvent treatment [11,12]. Unwanted materials are also separated from UCO using centrifugation, chromatography methods, vacuum filtration, mechanical precipitation, activated charcoal, and resin binders [13]. Conventional methods still have several disadvantages, such as the need for large amounts of chemicals, the creation of byproducts, and high infrastructure costs, even though some contaminants can be removed fairly successfully. These obstacles are among the factors that make the UCO conversion process less successful [2]. As a result, a different pretreatment strategy is required that can concurrently address these problems with minimal additional waste and with potential scalability.

Photocatalysis enables the generation of active radicals ($\cdot OH$, $\cdot O_2^-$, h^+) that can oxidise and decompose complex organic molecules into simpler, less toxic materials without introducing significant amounts of chemical impurities [14]. This process uses semiconductor materials activated by light to produce electron-hole pairs that can trigger redox reactions [15]. Titanium oxide (TiO_2) is a semiconductor material that is widely used for the degradation of various organic compounds, including phenol [16], diesel oil [17], and the methylene blue dye [18]. Nevertheless, TiO_2 can only absorb ultraviolet light, so it readily undergoes electron-hole recombination and has a large band gap. In a bid to overcome some of those challenges, TiO_2 is doped with other metal oxides to form composites that absorb more light and increase charge separation. Metal oxides, such as zinc oxide (ZnO) and cupric oxide (CuO), can be employed as dopants with TiO_2. TiO_2/CuO and TiO_2/ZnO composites exceed commercially available TiO_2 in the imazipyr degradation rate [19]. Collectively, TiO_2/ZnO/CuO degrades diazinon by 91% [20].

In addition to the composition of its constituent materials, the performance of photocatalysts is also influenced by the structure and morphology of the catalyst. Appropriate structure and morphology can facilitate electron transfer and enhance optical absorption, thereby improving photocatalyst performance [21,22]. Recently, many researchers have used surfactants to modify catalyst morphology. Hydrophilic and hydrophobic groups in surfactant can act as shape-directing agents in photocatalyst synthesis. Surfactants have been used to alter photocatalysts, including both single particles, such as ZnO [23], and composite materials, such as TiO_2-CNT [24]. HDTMA-Br is a type of cationic surfactant commonly used in composite morphology modification. Previous studies have reported that HDTMA-Br can reduce agglomeration and enhance the dispersion of CuO/TiO_2 nanocomposites, thereby increasing their photocatalytic activity [25].

Based on this framework, this study developed and evaluated the performance of HDTMA-Br-modified TiO_2/ZnO/CuO photocatalysts for the degradation of oxidative components in UCO, such as free fatty acids and peroxide compounds. This study examines the impact of adding HDTMA-Br surfactant on the morphological structure and performance of a TiO_2/ZnO/CuO photocatalyst for the degradation of oxidative compounds in UCO. Furthermore, discuss the degradation mechanism and the types of radicals involved, as well as testing the effectiveness of the photocatalyst system's operating conditions. This study proposes an alternative solution to enhance the processing of UCO waste into a high-value product in countries such as Indonesia, a significant oil producer. It addresses the limitations of conventional methods in reducing oxidative compounds that compromise the quality and safety of downstream products.

2. Materials and Methods

2.1 Materials and Instruments

The materials used in this study were used cooking oil (UCO), potassium hydroxide (KOH, Merck), zinc chloride ($ZnCl_2$, Merck), titanium oxide (TiO_2, Merck),

copper nitrate ($Cu(NO_3)_2$, Merck), hexadecyltrimethylammonium bromide (HDTMA-Br, Merck), hydrochloric acid (HCl, Smart Lab), sodium hydroxide (NaOH, Merck), potassium hydrogen phthalate ($C_8H_5KO_4$, Merck), sodium thiosulfate pentahydrate ($Na_2S_2O_3.5H_2O$, Merck), potassium dichromate ($K_2Cr_2O_7$, Smart Lab), potassium iodide (KI, Merck), acetic acid (CH_3COOH, Merck), ethanol (C_2H_6O, Merck), isooctane (C_8H_{18}, Merck), isopropanol (C_3H_8O, Merck), 1,4-benzoquinone ($C_6H_4O_2$, Merck), phenolphthalein indicator ($C_{20}H_{14}O_4$, Merck), starch indicator ($(C_6H_{10}O_5)_n$, Merck), hexane (C_6H_{14}, Merck), potassium bromide (KBr, Merck), and distilled water. All chemicals are used as is without further purification.

The instruments used to characterize the synthesized composites include SEM (COXEM EM-40), XRD (Rigaku MiniFlex 300/600), BET (QuadraSorb Station 2 version 7.01), FTIR (Shimadzu Prestige-21), and UV-DRS (PerkinEmler Lambda 365+).

2.2. Synthesis of HDTMA-Br Modified TiO_2/ZnO/CuO Composite

A total of 0.05 mol of TiO_2, 0.05 mol of $ZnCl_2$, and 0.025 mol of $Cu(NO_3)_2$ were added to 600 ml of distilled water. After homogenization, 0.5, 1, and 2 CMC HDTMA-Br were added, and the mixture was stirred for 30 minutes to achieve homogeneity. A 0.05 M NaOH solution was added slowly while stirring at 750 rpm for 1 hour, until the system reached pH 12. The solution was left to stand until a precipitate formed. The resulting precipitate was washed several times with distilled water until the pH was neutral. The remaining water in the precipitate was removed by heating in an oven at 105 °C. The dried precipitate was then calcined at 450 °C for 4 hours. A similar procedure was also carried out for the control sample, which was not added with HDTMA-Br.

2.3. Characterization of Synthesized TiO_2/ZnO/CuO Composite

X-ray diffraction (XRD) characterization was performed over a 2θ range of 5–90° with a step size of 0.01° and a data acquisition rate of 10°/min. Each composite morphology was observed using a scanning electron microscope (SEM), which recorded and generated images at 2,000x magnification and 18 kV. Using the KBr (potassium bromide) technique, FTIR (Fourier Transform Infrared Spectroscopy) was used to determine the number and type of functional groups in the pellets, using a 99:1 (by weight) ratio in the range of 4000 to 400 cm^{-1}. The composites were also characterized using nitrogen gas adsorption and desorption techniques, including the Brunauer-Emmett-Teller (BET) and Barrett-Joyner-Halenda (BJH) methods, to determine their textural properties. Optical studies were performed using ultraviolet-visible diffuse reflectance (UV-DRS) spectroscopy to determine the bandgap energy of the composites.

2.4. Photodegradation of UCO

The photodegradation reaction was carried out in a 250 mL beaker on a hot plate. The system was placed in a black box measuring 80 cm × 30 cm × 40 cm, equipped with a 16 Watt visible-light lamp and a 16 Watt ultraviolet lamp. The reaction was carried out at 120 °C for 60 minutes, using a 5% photocatalyst concentration relative to the oil mass (100 g). Degradation was also carried out under dark conditions (without light) as a comparison. The degradation reaction was carried out at a stirring speed of 750 rpm. After photocatalytic treatment, the suspension was allowed to stand under static conditions for 24 hours to ensure complete catalyst sedimentation. The %FFA and peroxide value of the photodegraded oil were then calculated before and after degradation. FFA was calculated by alkalimetric titration [26], while the peroxide value was calculated by oxidoreductometric titration [27].

2.5. Optimization of UCO Photodegradation Conditions

Optimization was performed at varying times (0.5, 1, 1.5, and 2 hours) and temperatures (27, 60, 90, and 120 °C). In addition, photodegradation was carried out

with varying surfactant concentrations (0, 0.5, 1, and 2 times the critical micelle concentration (CMC) of HDTMA-Br). The CMC of HDTMA-Br is known to be 0.9 mM at 25 °C [28].

2.6. Radical Scavenger Test in Photodegradation

The main radical species involved in photodegradation were identified by adding radical scavengers to the photodegradation system. Na-EDTA was added to scavenge holes (h^+), isopropanol to scavenge $\cdot OH^-$ radicals, and 1,4-benzoquinone to scavenge $\cdot O_2^-$ radicals. Each photodegradation system with added radical scavengers was reacted at 120 °C for 1 hour at 750 rpm. The photodegraded oil with scavengers was also measured for %FFA and peroxide value to determine which radical was dominant in the reaction.

2.7 Catalyst Recovery

After photodegradation is complete, the precipitated catalyst is washed with hexane to remove any remaining oil. It is then washed again with ethanol to remove any remaining polar compounds adhering to the catalyst pores. The composite is dried in an oven at 100°C until dry for reuse.

3. Results and Discussion

3.1. Characterization of TiO_2/ZnO/CuO Composite

The FTIR spectrum of the resulting TiO_2/ZnO/CuO composite is shown in Figure 1, where the vibration band indicating the presence of Zn–O bonds appears at around 425 cm^{-1} [29]. A typical absorption peak for the Cu–O bond is detected at around 529 cm^{-1}. TiO_2 group contributes to the formation of the band at 1024 cm^{-1}, which is related to the O–Ti–O bridging mode, and the band around 780 cm^{-1} marks the Ti–O–Ti stretching vibration [30]. The presence of Zn gives rise to an absorption signal at around 675 cm^{-1}, which is related to the vibrational mode of the Zn–O–Ti group [31]. This absorption indicates the formation of a composite oxide of TiO^2 and ZnO, not just a physical mixture. The signal at 1250 cm^{-1} indicates the presence of lattice vibrations in the TiO_2 structure. The strong bending vibration that appears at 1480 cm^{-1} is the absorption of titanol υ (Ti–OH) and water molecules [32]. The 1634 cm^{-1} absorption peak also shows Ti–OH bending absorption [33].

The O–H stretching vibration is displayed in the range of 3350–3430 cm^{-1}, while the band around 1630–1635 cm^{-1} is related to the bending mode of the H–O–H molecule, which comes from the adsorption of water vapor or moisture on the sample surface during the sampling process [29]. The O–H deformation and stretching bands at around 1635 cm^{-1} indicate that the composite surface has a certain degree of hydroxylation, which allows reaction with holes formed during photocatalysis, thereby inhibiting the recombination of electron–hole pairs [34,35]. The FTIR spectrum also displays an absorption band at 3700 cm^{-1}, attributed to isolated OH groups (Ti–OH) on the anatase (101) and (001) planes, indicating the presence of defects or oxygen vacancies on the composite surface [35,36]. In addition to the main peak, a CO_2 absorption band was also detected at 2343 cm^{-1} due to the high humidity during the analysis. There were no peak differences between the 0 CMC and 1 CMC composite spectra. This proves that no surfactant residues were found on the 1 CMC catalyst.

Two types of composites were analyzed by XRD, namely TiO_2/ZnO/CuO without surfactant modification (0 CMC) and TiO_2/ZnO/CuO with HDTMA-Br 1 CMC surfactant modification. From Figure 2, sharp, prominent peaks corresponding to each phase are visible. These sharp peaks indicate the successful synthesis of the three main components in crystalline form. The phases produced from the 0 and 1 CMC composites were anatase (TiO_2) based on ICDD No. 89-4921, zincite (ZnO) based on ICDD No. 36-1451, and tenorite (CuO) based on ICDD No. 04-0477. The anatase TiO_2 phase exhibits better activity than rutile due to its slightly longer electron and hole lifetimes [37]. In addition, the zincite ZnO phase and tenorite CuO phase are the

best phases with crystal stability, energy band position, and favorable charge absorption/transfer capabilities [38].

The Scherrer equation results confirm that each phase is in the nanometer range. The average crystallite size of the 0 CMC composite was determined to be 29.79 nm, with a crystallinity of 72.52%. In contrast, the 1 CMC catalyst had an average crystallite size of 29.63 nm and a crystallinity value of 74.54%. Modification with surfactants decreased the crystallite size but increased the crystallinity, consistent with the findings of Estrada-Flores *et al.* [35]. The resulting composite is classified as highly crystalline due to the elimination of grain boundary defects during the high-temperature calcination stage (450 °C) for 4 hours. At this temperature, the dominant anatase phase of TiO_2 forms, which is highly desirable due to its excellent photocatalytic properties [37]. In addition to the architectural phase, other factors, such as crystallinity and crystallite size, also affect photocatalytic activity [39]. The enhanced crystallinity of a particular photocatalyst increases its effectiveness in degrading organic compounds.

The surface area, pore size, and pore volume analysis of TiO_2/ZnO/CuO composites were performed using the BET–BJH method. The adsorption–desorption curves of CMC 0 and 1 composites (Figure 3) showed that the catalyst followed a type IV isotherm with a mesoporous structure characterized by the appearance of hysteresis in the partial pressure range of 0.6–0.9 [40,41]. The BET–BJH results (Table 1) showed that modifying TiO_2/ZnO/CuO with HDTMA-Br at 1 CMC significantly increased the specific surface area and total pore volume. In contrast, the average pore size slightly decreased to 3.87 nm. This increase in surface area and pore volume is consistent with the formation of a more developed mesoporous network due to the addition of surfactants during precipitation and calcination. At CMC concentrations, the cationic surfactant HDTMA-Br acts as a soft template, forming a gel/precipitate during drying. After calcination, the organic part of the surfactant degrades, leaving mesoporous cavities. This phenomenon is consistent with the increase in the N_2 adsorption capacity and the formation of hysteresis in the isotherm. This finding is consistent with the report of Kachbouri *et al.* [42], which showed that modification with the cationic surfactant CTAB can increase the specific surface area and total pore volume of TiO_2 particles.

The optical properties of the composite were characterized using UV–Vis DRS. The UV–Vis DRS spectrum of the TiO_2/ZnO/CuO composite in Figure 4 shows high absorption intensity in the UV region (220–380 nm), which is an intrinsic band transition of wide bandgap semiconductors such as TiO_2 and ZnO. In addition, absorption in the visible region (~650 nm) was observed, which is characteristic of CuO. The integration of TiO_2, ZnO, and CuO into a single composite has been shown to broaden the light absorption range from the visible to the ultraviolet region. The addition of ZnO also increases the number of active sites on the catalyst surface. Conversely, the presence of CuO functions as a cocatalyst, extending charge separation time by increasing electron and hole transfer rates [43].

The band gap energy of TiO_2/ZnO/CuO composites was determined through Tauc plot analysis and Kubelka Munk function. Figures 5 and 6 show Tauc plots for direct and indirect transitions of the synthesized composites, with the characteristic differences between the 0 and 1 CMC samples. In the 0 CMC sample, both approaches yield the same band gap of 2.73 eV. The 1 CMC sample shows a slight increase in the band gap value to 2.82 eV for the direct transition and 2.90 eV for the indirect transition. The band gap of the synthesized composite is lower than that of single ZnO (3.2 eV) [44] and single TiO_2 (3.12 eV) [32]. The smaller crystallite size of the 1 CMC composite, as determined by XRD, is in line with the slightly larger band gap of 1 CMC. A small particle size decreases the dimension, making the energy levels discrete and ultimately increasing the band gap energy [28].

Figure 7 SEM micrograph at 2,000× magnification shows apparent morphological differences between the TiO_2/ZnO/CuO 0 and 1 CMC samples. The 0 CMC sample displays relatively large coarse agglomerates and wide inter-aggregate gaps. The smaller, more uniform particle size in the 1 CMC sample is consistent with

the findings reported by Fatika *et al.* [45]. The surfactant added to the 1 CMC composite serves as a micelle template, thereby facilitating the formation of a porous surface after calcination [46]. Surfactants also act as mesostructure-directing agents and inhibit the growth of composite crystals during calcination, resulting in smaller, more uniform particle sizes [47,48]. Although surfactants have degraded during calcination, as evidenced by the absence of organic peaks in the FTIR spectrum, their impact as templating agents on morphology, such as pore size and catalyst crystallinity, persists [49]. The SEM observations are consistent with the BET–BJH and XRD analyses, which show that modification with HDTMA-Br can increase the specific surface area and pore volume while reducing the particle and pore sizes of the composite.

3.2. UCO Photodegradation Performance

Photodegradation experiments using TiO_2/ZnO/CuO composites demonstrated the ability to reduce free fatty acid (FFA) levels and peroxide values. Figure 8 presents the performance of the photocatalyst in reducing the FFA and peroxide rates in each system after 1 hour of photodegradation at 120 °C with a catalyst concentration of 5%. The results indicate that in the dark treatment (without UV–Vis irradiation), the decrease in FFA and peroxide values still occurs due to the adsorption of free fatty acids and hydroperoxides on the catalyst surface [50]. The photocatalytic process (with UV–Vis irradiation) exhibited superior performance, indicating that, in addition to adsorption, the catalyst surface also facilitates heterogeneous reactions that generate radical species ($\cdot OH$, $O2^{-}\cdot$, h^{+}) capable of decomposing oxidation products and organic components. Consistent with previous findings by Kaltsum *et al.* [51], TiO_2 thin films can also reduce the percentage of free fatty acids and peroxide values.

3.3. Optimization of UCO Photodegradation Conditions

The effect of photodegradation time on the reduction of FFA and peroxide values in UCO has been thoroughly studied (Figure 9). In the 0.5 to 1 hour interval, a sharp decrease in FFA occurs, with the maximum reduction at 1 hour, approximately 65% of the initial value before treatment. After 1.5 hours, photodegradation performance decreases due to a reduction in the number of active sites on the catalyst, thereby reducing the efficiency of triglyceride photolysis. In the initial phase of the process (0–1 hour), the high availability of active sites and the abundant substrate concentration allow the formation of reactive radicals ($\cdot OH$, $\cdot O_2^{-}$), which cause intense oxidation. After 1 hour, secondary oxidation and degradation products form, which can cover the catalyst's active site, thereby inhibiting interaction between the substrate and the active site [52]. The photodegradation performance of peroxide continues to increase after 1 hour due to photooxidation, which converts peroxide into secondary oxidation products. Thus, 1 hour can be considered the optimal time for the TiO_2/ZnO/CuO composite to degrade FFA and peroxide in UCO effectively.

Increasing the reaction temperature has been shown to affect the performance of UCO photodegradation significantly. Increasing the temperature from 27 °C to 60 °C, 90 °C, and 120 °C in Figure 10 shows a consistent relationship with the photocatalyst's increasing effectiveness in reducing FFA and peroxide levels in used cooking oil. The catalysis system at high temperatures not only improves decomposition efficiency but also reduces viscosity and mass transfer resistance, thereby increasing the collision frequency between the catalyst and the reactants [4]. However, the reaction is not carried out at temperatures exceeding 120 °C because unsaturated triglycerides in the oil can react with oxygen or water vapour in the environment, altering viscosity and increasing acidity [53]. Heating at very high temperatures also triggers the oxidative degradation of triglycerides, producing diglycerides, FFA, and lower-molecular-weight triglycerides. In addition, oils with lower levels of fatty acid saturation tend to undergo more intense oxidative

degradation; therefore, high-temperature thermal processing should be avoided to prevent measurement bias [54]. Based on these findings, the optimum temperature for the UCO photodegradation process using the TiO_2/ZnO/CuO composite is 120 °C.

The effect of surfactant concentration on the reduction in FFA and UCO peroxide values in the composite is shown in Figure 11. A surfactant concentration of 1 CMC showed the best performance compared to 0, 0.5, and 2 CMC. Previous research by Fatika *et al.* [45] reported that surfactant concentrations exceeding the CMC yield larger particle sizes than in unmodified composites, thereby reducing the photodegradation performance of UCO. In addition, surfactant concentrations above the CMC can form a bilayer that covers the catalyst's active sites.

3.4. Types of Active Radicals in UCO Photodegradation.

To identify the reactive oxygen species (ROS) that dominate the photocatalytic process, radical scavenging experiments were conducted. In these experiments, EDTA-2Na, isopropanol, and 1,4-benzoquinone were used as hole (h^+), hydroxyl radical (·OH), and superoxide radical ($\cdot O_2^-$) scavengers, respectively [50,55]. According to Figure 12, the percentage degradation decreased in each system after the addition of radical scavengers because these radicals could no longer participate in the oxidative reactions required for compound degradation. The trapped radicals could not be converted to $^1O_2$, thus limiting the formation of oxidative compounds and resulting in suboptimal degradation. However, several alternative reaction pathways were still possible, resulting in a relatively low overall degradation rate [52]. Figure 12 also shows that ·OH radical scavenging inhibited the reduction of FFA and peroxide values more significantly than other radical types. This suggests that ·OH radicals play an essential role in the photodegradation mechanism of UCOs in these systems. OH• radical is the most reactive radical in biological systems [56]. The findings of Trenczek-Zajac *et al.* [57] also confirmed that ·OH radical plays an essential role in the photodegradation of rhodamine blue dye using TiO_2 photocatalyst. Meanwhile, $\bullet O_2^-$ radical and h^+ hole act as secondary radicals that contribute to the photocatalytic reaction in this system.

3.5 Band Alignment and Heterojunction in TiO_2/ZnO/CuO Composite

For an effective and efficient photocatalytic reaction, in addition to preventing electron-hole recombination, the position of the catalyst band edge must match the oxidation and reduction redox potentials of water or oxygen. The valence band edge (VB) must be more positive than the water redox potential. The conduction band edge (CB) of the material must be more negative than the oxygen redox potential [58]. Based on radical-scavenging experiments, hydroxyl radicals (·OH) were identified as the dominant reactive species responsible for the degradation of used cooking oil. To rationalize the origin of ·OH formation and its relationship to charge separation in the TiO_2/ZnO/CuO system, data on the valence and conduction band potentials of each oxide constituent of the composite are required. The positions of the valence band edge (E_{VB}) and conduction band (E_{CB}) at pH 7 (vs. NHE) for TiO_2, ZnO, and CuO were determined using the Mulliken electronegativity method in Equations 1 and 2.

$$E_{VB} = x - E_C + {}^1/_2\, E_g \quad (1)$$

$$E_{CB} = E_{VB} - E_g \quad (2)$$

Where x represents the absolute electronegativity of the material, Ec is the free electron energy on the hydrogen scale (4.5 eV), and Eg is the band gap energy obtained from UV–Vis DRS analysis. The absolute electronegativity values are 5.895 eV for TiO_2, 5.81 eV for ZnO, and 5.81 eV for CuO, respectively. The band gaps of the oxide semiconductors are TiO_2 (3.15 eV), ZnO (3.20 eV), and CuO (1.39 eV). Using these parameters, the calculated E_{VB}/E_{CB} values are +2.97 eV / -0.18 eV for TiO_2, +2.91 eV / -0.29 eV for ZnO, and +2.01 eV / +0,62 eV for CuO (vs. NHE at pH 7) [59,60].

These values define the band alignment depicted in Figure 13. Assuming pH 7 is consistent with the Mulliken electronegativity method, as commonly reported in the literature for gas-phase photocatalytic systems [61].

The valence band potentials of TiO_2 (+2.97 eV vs. NHE) and ZnO (+2.91 eV vs. NHE) are more positive than the redox potential of $H_2O/ \cdot OH$ (+2.27 eV vs. NHE). The VB potentials of TiO_2 and ZnO, which are more positive than the water potential, indicate that these materials can thermodynamically oxidize water or hydroxide ions to produce hydroxyl radicals. Furthermore, electrons in the conduction bands of TiO_2 and ZnO (-0.18 eV and -0.29 eV vs. NHE) play a role in the reduction of oxygen to $\cdot O_2^-$ because they are more negative than the oxygen potential, which is -0.046 eV. The valence and conduction bands of CuO are insufficient for the direct formation of OH and $\cdot O_2^-$. The narrower band gap of CuO allows CuO to act as an electron acceptor, facilitating charge separation and suppressing electron-hole recombination. The optimized energy structure facilitates more efficient charge separation and enhances photocatalytic activity [62]. The proposed TiO_2/ZnO/CuO heterojunction mechanism is the Z-scheme. The TiO_2 conduction band (CB) is more negative than the CuO conduction band, facilitating effective electron transfer from the TiO_2 CB to the CuO CB. At the same time, there is an energy level difference between the CuO conduction band and the ZnO valence band (VB). This energy difference facilitates electron transfer from the CuO CB to the ZnO VB, where the electrons accumulate. This electron movement prevents internal recombination within the composite material, thereby extending the lifetimes of h^+ and e^-, ultimately improving photocatalytic performance. In the TiO_2/ZnO/CuO composite, oxygen reduction to superoxide radicals ($\cdot O_2^-$) occurs in the ZnO CB, while water oxidation to hydroxyl radicals ($\cdot OH$) occurs in the TiO_2 VB.

3.6. Mechanistic Study of UCO Photodegradation

The photocatalytic degradation of UCO oxidative compounds using TiO_2/ZnO/CuO photocatalysts involves the formation of free radicals. The radicals formed will react with carboxylic acids (free fatty acids). Additionally, with the aid of light or heat, the generated radicals will start bond cleavage, ring opening, hydroxylation, and ketolysis reactions, creating intermediates before final mineralization to carbon dioxide and water. Hydroxyl radicals are the primary radicals at TiO_2/ZnO/CuO to degrade UCO oxidative compounds. These radicals produce carbon dioxide, water, and organic radicals ($R \cdot CH_2$) when they interact with carboxylic acid groups (free fatty acids). Organoperoxy radicals ($RCH_2OO \cdot$) are created when the generated organic radicals interact with oxygen molecules. As illustrated in Figure 14, organoperoxy reacts with hydroperoxy radicals ($\cdot OOH$) to form organohydroperoxides (RCH_2OOOOH), which are subsequently mineralized to produce water, carbon dioxide, and alcohol [63,64]. Hydroperoxyl radicals are radicals formed from a second oxygen molecule reacting with H^+ and electrons from photocatalysis. In a photocatalytic reaction, the absorbed photon activates two oxygen molecules, one of which ultimately forms a hydroperoxyl radical [65].

3.7. Catalyst Cycle

The catalytic cycle is an essential parameter in evaluating photocatalyst performance. In this study, four catalytic cycles were carried out. The catalyst after the first cycle was reused to degrade FFA and peroxide on fresh UCO. Figure 15 shows the performance of the 2 CMC photocatalyst in four cycles. The 2 CMC composite with a relatively high surfactant concentration can partially block the active sites. This composite at 2 CMC was deliberately chosen in the catalytic cycle to assess the robustness and structural stability of the TiO_2/ZnO/CuO composite. In Figure 15, photodegradation performance decreases slightly with increasing cycles. The reduction in photocatalytic activity is attributable to surface fouling or partial

coverage by organic residues and surfactants. The decline in performance is not attributable to structural degradation of the catalyst, as the catalyst retains a robust structure after four cycles, as shown in Figure 16.

Figure 16 compares the XRD patterns of the TiO_2/ZnO/CuO-HDTMA-Br photocatalyst before use and after four consecutive photocatalytic cycles. The XRD pattern after four consecutive cycles shows no emergence of new crystalline phases and no significant peak shifts, indicating that the crystal structures of TiO_2 (anatase), ZnO, and CuO remain intact. A slight decrease in peak intensity and minor peak broadening are observed for the reused catalyst compared with the fresh catalyst. This phenomenon is likely due to partial structural reorientation induced by repeated photocatalytic cycles and heating at 100° C [66]. Nevertheless, the presence of the major TiO_2, ZnO, and CuO phases indicates that the composite framework is preserved mainly after multiple reuse cycles, thereby ensuring its structural integrity.

The presence of all major crystalline phases after four cycles demonstrates that the TiO_2/ZnO/CuO-HDTMA-Br photocatalyst has excellent phase stability and resistance to structural collapse. This structural robustness is a crucial factor supporting the reusability and feasibility of catalyst engineering, particularly for practical applications. Furthermore, the TiO_2/ZnO/CuO-HDTMA-Br photocatalyst was easily separated from UCO by sedimentation for 24 hours without the need for additional instruments. The separated catalyst also exhibited a high recovery rate (>88%). From an engineering perspective, this low-energy and straightforward method enhances the practical application of photocatalytic pretreatment processes for used cooking oil.

4. Conclusions

TiO_2/ZnO/CuO-HDTMA-Br composite has been successfully synthesized through precipitation. 1 CMC modification produces a catalyst with increased specific surface area, increased pore volume, and increased crystallinity, which in turn supports the photodegradation performance of UCO. Photodegradation of UCO with TiO_2/ZnO/CuO composite successfully reduced the amount of FFA and peroxide up to a maximum of 65% for FFA and 59% for peroxide. The optimal conditions for UCO photodegradation were achieved at a reaction time of 1 hour, a temperature of 120 °C, and a surfactant concentration in the catalyst of 1 CMC. The photodegradation reaction of UCO involves a radical process, with hydroxyl radicals (·OH) being the main radical in this system. This study can serve as the first step and basis for UCO pretreatment, with a primary focus on reducing FFA and peroxide compounds. Further research is needed to process the photodegraded oil into downstream products and then compare their quality with those made from UCO without degradation pretreatment.

5. Acknowledgement

We thank the Department of Chemistry at Bogor Agricultural University for its support of this research. We also thank Pertamina Research and Technology Innovation for their assistance in the XRD analysis of the research samples.

6. Credit Author Statement

Author Contributions: Each author contributed to the manuscript. Komar Sutriah served as the research coordinator, conceived the study, and provided material support. Mohammad Khotib and Sri Mulijani provided material support and advice during the study. Adinda Pitaloka conceived the study, prepared the materials, collected the data, and processed and analyzed it. She also wrote the draft manuscript,

assisted by comments and suggestions from all authors. All authors have read and approved the published version of the manuscript.

7. References

[1]. USDA Foreign Agricultural Service (FAS). (2025). *Oilseeds: World Markets and Trade*. United States Department of Agriculture. Available at https://www.fas.usda.gov/data/oilseeds-world-markets-and-trade-03082024

[2]. Awogbemi, O., Kallon, D. V. V. (2024). Conversion of Hazardous Waste Cooking Oil into Non-Fuel Value Added Products. *International Journal of Ambient Energy*, 45. DOI: 10.1080/01430750.2024.2345253.

[3]. Ambreen, G., Siddiq, A., Hussain, K. (2020). Association of Long-Term Consumption of Repeatedly Heated Mix Vegetable Oils in Different Doses and Hepatic Toxicity Through Fat Accumulation. *Lipids Health*, 19, 69. DOI: 10.1186/s12944-020-01256-0.

[4]. Guo, M., Jiang, W., Ding, J., Lu, J. (2022). Highly Active and Recyclable CuO/ZnO as Photocatalyst for Transesterification of Waste Cooking Oil to Biodiesel and the Kinetics. *Fuel*. 315, 123254. DOI: 10.1016/j.fuel.2022.123254.

[5]. Teh, J. L., Walvekar, R., Ho, K. C., Khalid, M. (2025). Biolubricants from Waste Cooking Oil: A Review of Extraction Technologies, Conversion Techniques, and Performance Enhancement Using Natural Antioxidants. *Journal of Environmental Management*, 35, 124267. DOI: 10.1016/j.jenvman.2025.124267.

[6]. Hisham, N. H. M. B., Ibrahim, M. F., Ramli, N., Abd-Aziz, S. (2019). Production of Biosurfactant Produced from Used Cooking Oil by *Bacillus* sp. HIP3 for Heavy Metals Removal. *Molecules*, 24, 2617. DOI: 10.3390/molecules24142617.

[7]. Capello, M., Filippi, S., Rossi, D., Cinelli, D., Anguilessi, I., Camodeca, C., Orlandini, E., Polacco, G., Seggiani, M. (2024). Waste-Cooking-Oil-Derived Polyols to Produce New Sustainable Rigid Polyurethane Foams. *Sustainability*, 16, 9456. DOI: 10.3390/su16219456.

[8]. Zhang, N., Li, Y., Wen, S., Sun, Y., Chen, J., Gao, Y., Sagymbek, A., Yu, X. (2021). Analytical Methods for Determining the Peroxide Value of Edible Oils: A Mini-Review. *Food Chem*, 358, 129834. DOI: 10.1016/j.foodchem.2021.129834.

[9]. Farouk, S. M., Tayeb, A. M., Abdel-Hamid, S. M. S., Osman, R. M. (2024). Recent Advances in Transesterification for Sustainable Biodiesel Production, Challenges, and Prospects: A Comprehensive Review. *Environmental Science and Pollution Research International*. 31, 12722–12747. DOI: 10.1007/s11356-024-32027-4.

[10]. Manzocco, L., Romano, G., Calligaris, S., Nicoli, M.C. (2020). Modeling the Effect of the Oxidation Status of the Ingredient Oil on Stability and Shelf Life of Low-Moisture Bakery Products: The Case Study of Crackers. *Foods*. 9, 749. DOI: 10.3390/foods9060749.

[11]. Kurańska, M., Beneš, H., Prociak, A., Trhlíková, O., Walterová, Z., Stochlińska, W. (2019). Investigation of Epoxidation of Used Cooking Oils with Homogeneous and Heterogeneous Catalysts. *Journal of Cleaner Production*, 236, 117615. DOI: 10.1016/j.jclepro.2019.117615.

[12]. Nazrah H. R. S. F., Shahdan, S. N. (2021). Pre-treatment of Used Cooking Oil Followed by Transesterification Reaction in the Production of Used Cooking Oil-Based Polyol. *Scientific Research Journal,* 18, 129–146. DOI: 10.24191/srj.v18i2.13749.

[13]. Cárdenas, J., Orjuela, A., Sánchez, D. L., Narváez, P. C., Katryniok, B., Clark, J. (2021). Pre-treatment of Used Cooking Oils for the Production of Green Chemicals: A Review. *Journal of Cleaner Production*, 289, 125129. DOI: 10.1016/j.jclepro.2020.125129.

[14]. Zhu, L., Cheng, X., Cui, Y., Chen, F. (2024). Photocatalytic Activity and

Mechanism of $YMnO_3$/NiO Photocatalyst for the Degradation of Oil and Gas Field Wastewater. *Frontiers in Chemistry*, 12. DOI: 10.3389/fchem.2024.1408961.
[15]. Guo, M., Jiang, W., Chen, C., Qu, S., Lu, J., Yi, W., Ding, J. (2021). Process Optimization of Biodiesel Production from Waste Cooking Oil by Esterification of Free Fatty Acids Using La^{3+}/ZnO-TiO_2 Photocatalyst. *Energy Conversion and Management*. 229, 37–45. DOI: 10.1016/j.enconman.2020.113745.
[16]. Agustina, L., Romli, M., Suryadarma, P., Suprihatin, S. (2024). Green Synthesis of Titanium Dioxide Photocatalyst Using Lactobacillus bulgaricus for Processing Palm Oil Mill Effluent. *Global Journal of Environmental Science and Management*, 10, 13–26. DOI: 10.22034/gjesm.2024.01.01.
[17]. Lee, Y. J., Putri, L. K., Ng, B. J., Tan, L. L., Wu, T. Y., Chai, S. P. (2023). Blue TiO_2 with Tunable Oxygen-Vacancy Defects for Enhanced Photocatalytic Diesel Oil Degradation. *Applied Surface Science*, 611, 155716. DOI: 10.1016/j.apsusc.2022.155716.
[18]. Tichapondwa, S. M., Newman, J. P., Kubheka, O. (2020). Effect of TiO_2 Phase on the Photocatalytic Degradation of Methylene Blue Dye. *Physics and Chemistry of the Earth*, 118, 102900. DOI: 10.1016/j.pce.2020.102900.
[19]. Abdulfattah, I., El-Shamy, A. M. (2024). A Comparative Study for Optimizing Photocatalytic Activity of TiO_2-Based Composites with ZrO_2, ZnO, Ta_2O_5, SnO, Fe_2O_3, and CuO Additives. *Scientific Reports*, 14, 27175. DOI: 10.1038/s41598-024-77752-5.
[20]. Malakootian, M., Soori, M. M. (2021). Enhanced Photocatalytic Degradation of Diazinon by TiO_2/ZnO/CuO Nanocomposite under Solar Radiation. *Desalination and Water Treatment*, 242, 75–88. DOI: 10.5004/dwt.2021.27814.
[21]. Zhang, N., Wang, L., Wang, H., Cao, R., Wang, J., Bai, F., Fan, H. (2018). Self-Assembled One-Dimensional Porphyrin Nanostructures with Enhanced Photocatalytic Hydrogen Generation. *Nano Letters*, 18, 560–566. DOI: 10.1021/acs.nanolett.7b04701.
[22]. Li H., Sun, Y., Yuan, Z. Y., Zhu, Y. P., Ma, T. Y. (2018). Titanium Phosphonate Based Metalorganic Frameworks with Hierarchical Porosity for Enhanced Photocatalytic Hydrogen Evolution, *Angewandte Chemie International*, 57, 3222–3227. DOI: 10.1002/anie.201712925.
[23]. Yu, H., Wang, J., Yan, X., Wang, J., Cheng, P., Xia, C. (2019). Effect of Surfactants on the Morphology and Photocatalytic Properties of ZnO Nanostructures. *Optik*, 185, 990–996. DOI: 10.1016/j.ijleo.2019.04.040.
[24]. Heltina, D., Avisa, U., Fermi, M. I. (2021). The Role of Surfactant to Enhance Photocatalyst Performance on Phenol Degradation in TiO_2-CNT Composite-Modified CNT (Cetyltrimethylammonium Bromide). *IOP Conference Series: Materials Science and Engineering*. 1041. DOI: 10.1088/1757-899X/1041/1/012048.
[25]. Ravishankar, T. N., Vaz, M. O., Teixeira, S. R. (2020). The Effect of Surfactant on Sol-Gel Synthesis of CuO/TiO Nanocomposites for the Photocatalytic Activities under UV-Visible and Visible Light Illuminations. *New Journal of Chemistry*. 44, 1888–1904. DOI: 10.1039/C9NJ05246A.
[26]. ISO. (2020). *Animal and Vegetable Fats and Oils — Determination of Acid Value and Acidity*. ISO 660:2020.
[27]. ISO. (2017). *Animal and Vegetable Fats and Oils — Determination of Peroxide Value — Iodometric (Visual) Endpoint Determination*. ISO 3960:2017.
[28]. Rauf, H., Nodeh, H. R., Kareer, S., Aziz, M. (2019). Effect of Cationic Surfactants on Properties of Zinc Oxide Nanoparticles Synthesized through Sol-Gel Technique. *UHD Journal of Science and Technology*, 3, 93. DOI: 10.21928/uhdjst.v3n2y2019.pp93-107.
[29]. Uddin, M. J., Yeasmin, M. S., Muzahid, A. A., Rahman, M. M., Rana, G. M.,

Chowdhury, T. A., Amin, M., Wakib, M. K., Begum, S. H. (2024). Morphostructural Studies of Pure and Mixed Metal Oxide Nanoparticles of Cu with Ni and Zn. *Heliyon*. 10, 30544. DOI: 10.1016/j.heliyon.2024.e30544.
[30]. Yitagesu, G. B., Leku, D. T., Seyume, A. M., Workneh, G. A. (2024). Biosynthesis of TiO_2/CuO and its Application for the Photocatalytic Removal of the Methylene Blue Dye. *ACS Omega*. 9, 41301–41313. DOI: 10.1021/acsomega.4c03472.
[31]. Sawunyama, L., Oyewo, O., Onwudiwe, D. C., Makgato, S. S. (2023). Photocatalytic Degradation of Tetracycline Using Surface Defective Black TiO_2–ZnO Heterojunction Photocatalyst under Visible. *Heliyon*, 9, 11. DOI: 10.1016/j.heliyon.2023.e21423.
[32]. Mkhohlakali, A., Jen, T., Ledwaba, K., Mapukata, S., Mabowa, H. M., Letsoalo, M.R., Ntsasa, N., Tshilongo, J. (2024). Influence of Surfactant on Sol-Gel-Prepared TiO_2: Characterization and Photocatalytic Dye Degradation in Water. *Frontiers in Chemical Engineering*, 6. DOI: 10.3389/fceng.2024.1352283.
[33]. Behera, M., Al-qahtani, F. O., Chakrabortty, S., Nayak, J., Banerjee, S., Kumar, R., Jeon, B.H., Tripathy, S. (2023). CuO/TiO_2/ZnO NPs Anchored Hydrogen Exfoliated Graphene: To Comprehend the Role of Graphene in Catalytic Reduction of p-Nitrophenol. *ACS Omega*, 8, 42164–42176. DOI: 10.1021/acsomega.3c03859.
[34]. Ghorai, T., Chakraborty, M., Pramanik, P. (2011). Photocatalytic Performance of Nano-Photocatalyst from TiO_2 and Fe_2O_3 by Mechanochemical Synthesis. *Journal of Alloys and Compounds*, 509: 8158–8164. DOI: 10.1016/j.jallcom.2011.05.069.
[35]. Estrada-Flores, S., Martínez-Luévanos, A., Pérez-Berumen, C. M., García-Cerda, L. A., Flores-Guía, T. E. (2021). Relationship between Morphology, Porosity, and the Photocatalytic Activity of TiO_2 Obtained by Sol–Gel Method Assisted with Ionic and Nonionic Surfactants. *Boletín de la Sociedad Española de Cerámica y Vidrio*, 59, 209–218. DOI: 10.1016/j.bsecv.2019.10.003.
[36]. Amore, A., Filippone, F., Mattioli, G., Alippi, P. (2009). Oxygen Vacancies and OH Species in Rutile and Anatase TiO_2 Polymorphs. *Catalysis Today*, 144, 177–182. DOI:10.1016/j.cattod.2009.01.047.
[37]. Kim, M. G., Kang, J. M., Lee, J. E., Kim, K. S., Kim, K. H., Cho, M., Lee, S. G. (2021). Effects of Calcination Temperature on the Phase Composition, Photocatalytic Degradation, and Virucidal Activities of TiO_2 Nanoparticles. *ACS Omega*. 6, 10668–10678. DOI: 10.1021/acsomega.1c00043.
[38]. Dagareh, M. I., Hafeed, Y. H., Mohammed, J., Kavadi, A. D. G., Suleian, A. B., Ndikilar, C. E. (2024). Current Trends and Future Perspectives on ZnO-Based Materials for Robust and stable solar Fuel (H_2) Generation. *Chemical Physical Impact*. 9, 100774. DOI: 10.1016/j.chphi.2024.100774.
[39]. Nandianto, A. B. D., Zaen, R., Oktiani, R. (2020). Correlation between Crystallite Size and Photocatalytic Performance of Micrometer-Sized Monoclinic WO_3 Particles. *Arabian Journal of Chemistry*. 13, 1283–1296. DOI: 10.1016/j.arabjc.2017.10.010.
[40]. Cano-Casanova, L. A., Amorós-Pérez, M., Ouzzine, M. A., Lillo-Ródenas, L. R., Román-Martínez, M. C. (2018). One Step Hydrothermal Synthesis of TiO_2 with Variable HCl Concentration: Detailed Characterization and Photocatalytic Activity in Propene Oxidation. *Applied Catalysis*, 220, 645–653. DOI: 10.1016/j.apcatb.2017.08.060.
[41]. Abbad, M. M., Kadhum, A. A. H., Mohamad, A. B., Takriff, M. S., Sopian, K. (2012). Synthesis and Catalytic Activity of TiO_2 Nanoparticles for Photochemical Oxidation of Concentrated Chlorophenols under Direct Solar Radiation. *International Journal of Electrochemical Science*, 7, 4871–4888. DOI: 10.1.1.470.8294.
[42]. Kachbouri, S., Elaloui, E., Moussaoui, Y. (2018). The Effect of Surfactant

Chain Length and Type on the Photocatalytic Activity of Mesoporous TiO_2 Nanoparticles Obtained via Modified Sol-Gel Process. *Iranian Journal of Chemistry & Chemical Engineering-International*, 38, 17–26. DOI: 10.30492/ijcce.2019.29528.

[43]. Nishikori, H., Harata, N., Yamaguchi, S., Ishikawa, T., Kondo, H., Kikuchi, A., Yamakami, T., Teshima, K. (2019). Formation of CuO on TiO_2 Surface Using its Photocatalytic Activity. *Catalysts*, 9, 383–394. DOI: 10.3390/catal9040383.

[44]. Abhijit, A.R., Mashangva, T.T., Sharma, H., Srivastava, A., Thomas, R. (2025). Defect and Band Gap Engineering in Mg-Doped ZnO for Gas Sensing and Photocatalytic Applications. *Journal of Materials Science: Materials in Electronics*, 36, 1275. DOI: 10.1007/s10854-025-15532-1.

[45]. Fatika, S., Sutriah, K., Khotib, M. (2025). Synthesis and Characterization of HDTMA-Br Modified TiO_2/ZnO/CuO Photocatalyst Composite for Photodegradation of Textile Dye (Methyl Orange). *Jurnal Kimia Sains dan Aplikasi*, 28, 436–441. DOI:10.14710/jksa.28.8.436-441.

[46]. Wellia, D. V., Syafawi, A., Putri, Y. E., Muldarisnur, M. (2023). The Effect of Cetyltrimethylammonium Bromide (CTAB) Addition on Green Synthesis of Porous N-Doped TiO_2 for Photoreduction of Heavy Metal Ion Cr (VI). *RSC Advances*, 13, 29645–29656. DOI: 10.1039/D3RA03247G.

[47]. Bao, Y., Wang, T., Kang, Q., Shi, C., Ma, J. (2017). Micelle-Template Synthesis of Hollow Silica Spheres for Improving Water Vapor Permeability of Waterborne Polyurethane Membrane. *Scientific Reports*, 7, 1–14. DOI: 10.1038/s41598-016-0028-x.

[48]. Hamisu, A., Gaya, U.I., Abdullah, A.H. (2021). Bi-Template Assisted Sol-Gel Synthesis of Photocatalytically-Active Mesoporous Anatase TiO_2 Nanoparticles. *Applied Science and Engineering Progress*, 14. DOI: 10.14416/j.asep.2021.04.003.

[49]. Mendoza-Castro, M.J., Serrano, E., Linares, N., García-Martínez, J. (2020). Surfactant-Templated Zeolites: From Thermodynamics to Direct Observation. *Advanced Materials Interfaces*, 8, 2001388. DOI: 10.1002/admi.202001388.

[50]. Ogoh-Orch, B., Keatig, P., Ivaturi, A. (2023). Visible-Light-Active BiOI/TiO_2 Heterojunction Photocatalysts for Remediation of Crude Oil-Contaminated Water. *ACS Omega*, 8, 43556–43572. DOI: 10.1021/acsomega.3c04359.

[51]. Kaltsum, U., Kurniawan, A. F., Nurhasanah, I., Priyono, P. (2016). Reduction of Peroxide Value and Free Fatty Acid Value of Used Frying Oil Using TiO_2 Thin Film Photocatalyst. *Bulletin of Chemical Reaction Engineering and Catalysis*. 11, 369–375. DOI: 10.9767/bcrec.11.3.577.369-375.

[52]. Meng, Z., Peng, Z., Zhing, Q., Li, Y. (2025). Non-Radical Degradation Mechanism on ZnO Quantum Dots/Hollow-Sphere g-C_3N_4 S-Scheme Heterojunction Photocatalysts for Tetracycline Degradation. *Science*, 28, 113500. DOI: 10.1016/j.isci.2025.113500.

[53]. Tsai, Y. H., Chiang, D., Li, Y. T., Perng, T. P., Lee, S. (2023). Thermal Degradation of Vegetable Oils. *Foods*, 12, 1839. DOI: 10.3390/foods12091839.

[54]. Hu, Q., Zhang, J., He, L., Wey, L., Xing, R., Yu, N., Huang, W., Chen, Y. (2024). Revealing Oxidative Degradation of Lipids and Screening Potential Markers of Four Vegetable Oils During Thermal Processing by Pseudotargeted Oxidative Lipidomics. *Food Research International*, 175, 113725. DOI: 10.1016/j.foodres.2023.113725.

[55]. Li, D., Song, H., Meng, X., Shen, T., Sun, J., Han, W., Wang, X. (2020). Effects of Particle Size on the Structure and Photocatalytic Performance by Alkali-Treated TiO_2. *Nanomaterials (Basel)*, 10, 546. DOI: 10.3390/nano10030546.

[56]. Oh, W. Y., Kim, M. J., Lee, J. (2023). Approaches of Lipid Oxidation Mechanisms in Oil Matrices Using Association Colloids and Analysis

Methods for Lipid Oxidation. *Food Science and Biotechnology*, 32(13), 1805–1819. DOI: 10.1007/s10068-023-01359-1.

[57]. Trenczek-Zajac, A., Synowiec, M., Zakerzewska, K., Zazakowny, K., Kowalski, K., Dziedzic, A., Radecka, M. (2022). Scavenger-Supported Photocatalytic Evidence of an Extended Type I Electronic Structure of the TiO_2@Fe_2O_3 Interface. *ACS Applied Materials and Interfaces,* 14, 38255–38269. DOI: 10.1021/acsami.2c06404.

[58]. Abebe, B., Gupta, N. K., Tsegaye, D. (2024). A Critical Mini-review on Doping and Heterojunction Formation in ZnO-based Catalysts. *RSC Advances,* 14, 17338-17349. DOI: 10.1039/d4ra02568g.

[59]. Zhang, Y., Bo, X., Zhu, T., Zhao, W., Cui, Y., Chang, J. (2024). Synthesis of TiO_2-ZnO n-n Heterojunction with Excellent Visible Light-Driven Photodegradation of Tetracycline. *Nanomaterials*, 14(22), 1802. DOI:10.3390/nano14221802.

[60]. Ni, J., Lei, J., Wangm Z., Huang, L., Zhu, H., Liu, H., Hu, F., Qu, T., Yang, H., Gong, C. (2022). The Ultrahigh Adsorption Capacity and Excellent Photocatalytic Degradation Activity of Mesoporous CuO with Novel Architecture. *Nanomaterials*, 13(1), 142. DOI:10.3390/nano13010142.

[61]. Morante, N., Tammaro, O., Monzillo, K., Sannino, D., Battiato, A., Vittone, E., Castellino, M., Esposito, S., Vaiano, V. (2024). Unraveling the Role of CuO in CuxO/TiO_2 Photocatalyst for the Direct Propylene Epoxidation with O_2 in a Fluidized Bed Reactor. *Chemsuschem*. DOI: 10.1002/cssc.202401546.

[62]. Mohammed, S. O., Khalil, M. M. H., El-Sewefy, I. M., Radwan, A. (2025). Nd-doped CuO/ZnO and ZnO/CuO Heterojunctions for Simultaneous UV Blocking and Malachite Green Detoxification. *Scientific Reports*, 15, 34063. DOI: 10.1038/s41598-025-13945-w.

[63]. Nguyen, V. H., Phan, T. L. A., Van, Le. Q., Singh, P., Raizada, P., Kajitvichyanukul, P. (2020). Tailored Photocatalysts and Revealed Reaction Pathways for Photodegradation of Polycyclic Aromatic Hydrocarbons (PAHs) in Water, Soil, and Other Sources. *Chemosphere*, 260, 127529. DOI: 10.1016/j.chemosphere.2020.127529.

[64]. Yang, X., Cai, H., Bao, M., Yu, J., Lu, J., Li, Y. (2018). Insight into the Highly Efficient Degradation of PAHs in Water Over Graphene Oxide/Ag_3PO_4 Composites under Visible Light Irradiation. *Chemistry Engineering Journal*, 334, 355–376. DOI: 10.1016/j.cej.2017.09.104.

[65]. Heller, A. (1995). Chemistry and Applications of Photocatalytic Oxidation of Thin Organic Films. *Accounts of Chemical Research*, 28, 503–508. DOI: 10.1021/ar00060a006.

[66]. Albuquerque, W. A., Filho, A. J. N., Romaguera-Barcelay, Y., Medina-Carrasco, S., Orta, M. D. M., Trigueiro, P., Peña-Garcia, R. R. (2025). Synergistic ZnO–CuO/Halloysite Nanocomposite for Photocatalytic Degradation of Ciprofloxacin with High Stability and Reusability. *Minerals,* 15(9), 977. DOI:10.3390/min15090977.

FIGURE CAPTIONS

TABLE CAPTIONS

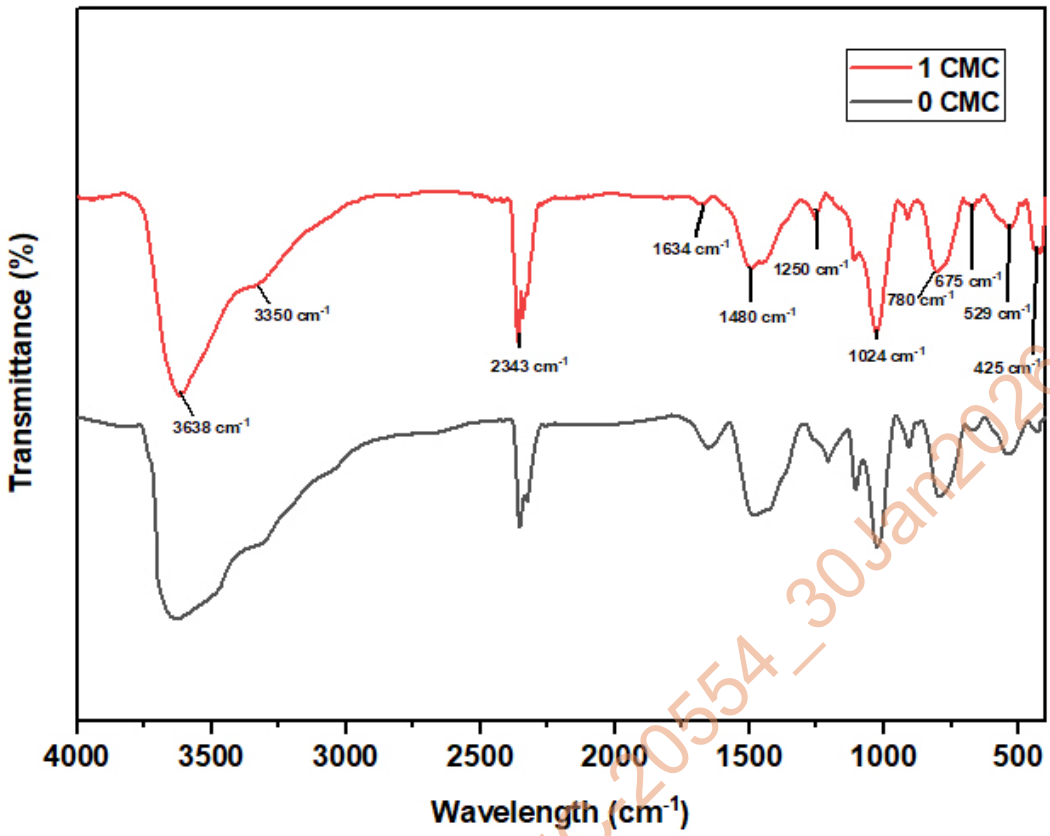

Figure 1. FTIR spectrum of TiO_2/ZnO/CuO 0 CMC and 1 CMC composites

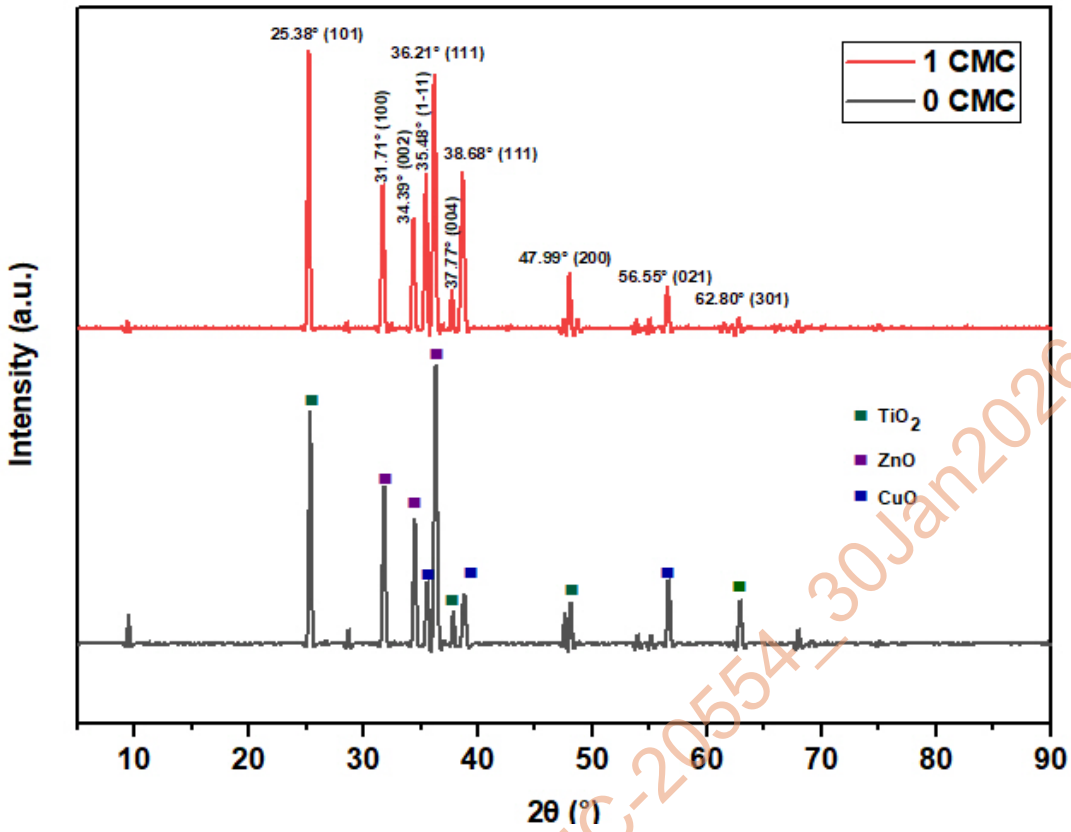

Figure 2. XRD spectrum of TiO_2/ZnO/CuO 0 CMC and 1 CMC composites

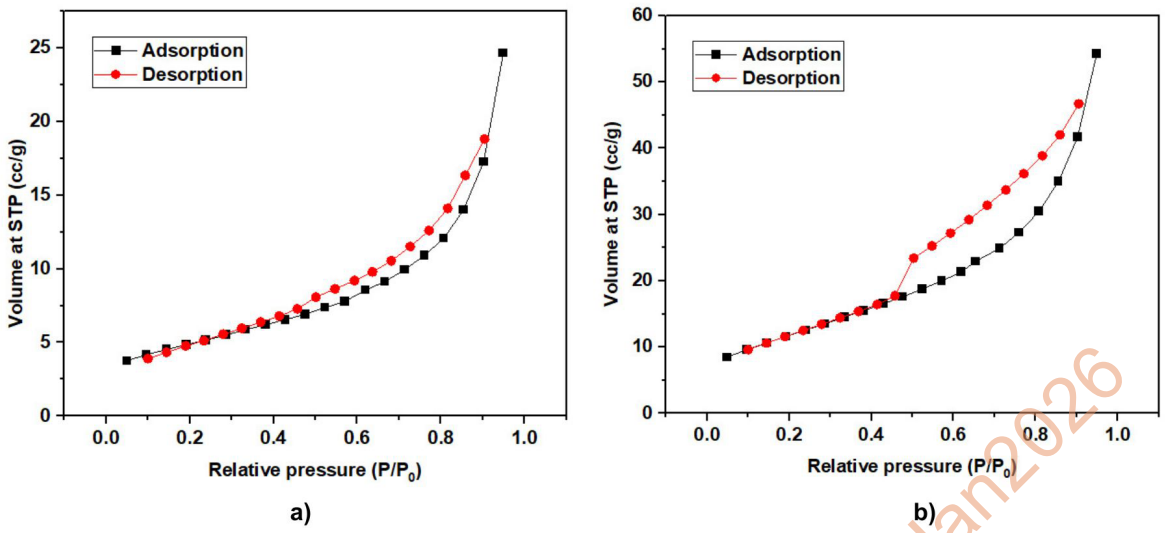

Figure 3. Adsorption-desorption isotherm curve of TiO_2/ZnO/CuO composites, a) 0 CMC and b) 1 CMC

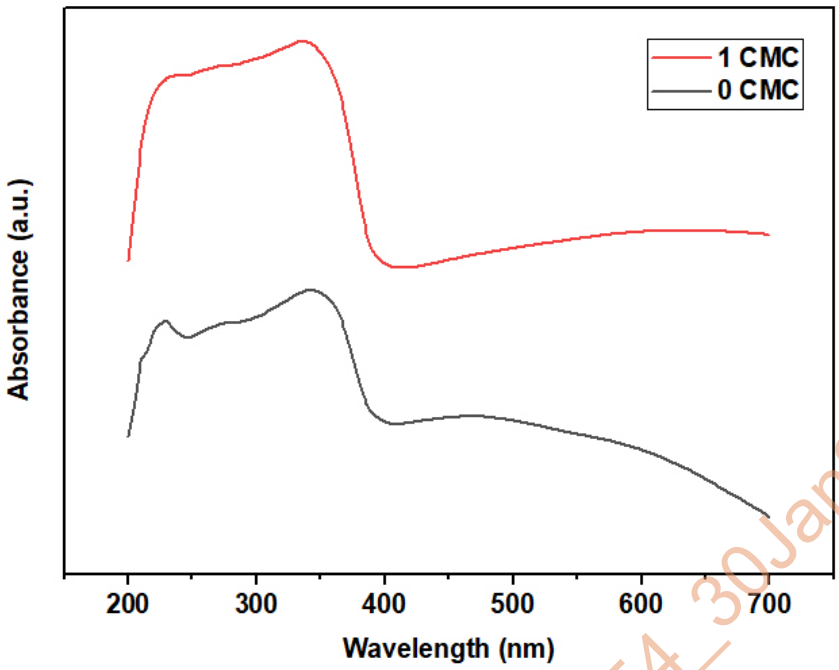

Figure 4. UV-Vis absorbance of TiO_2/ZnO/CuO 0 and 1 CMC composites

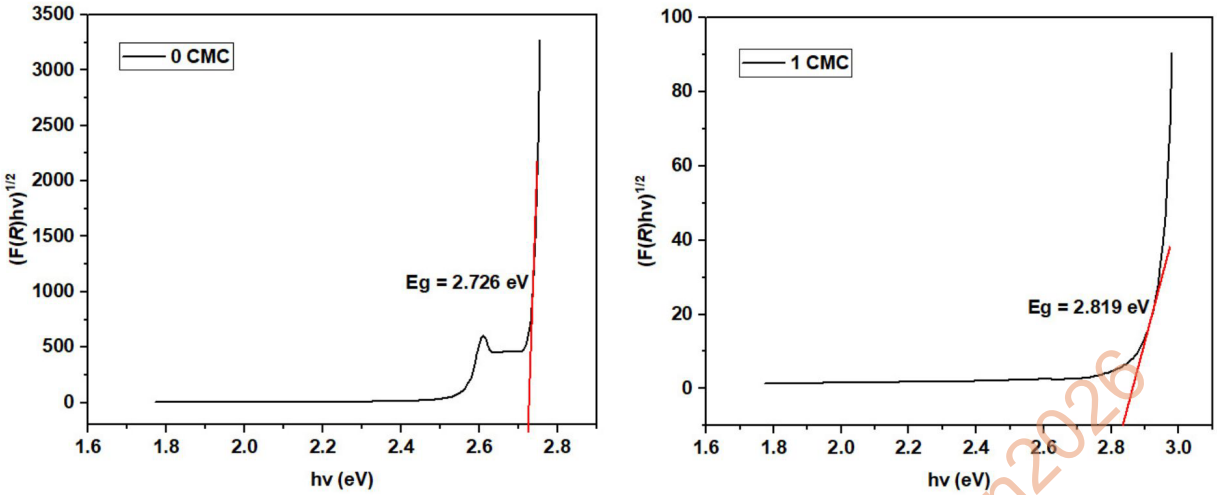

Figure 5. Tauc plot of indirect TiO_2/ZnO/CuO 0 and 1 CMC composites

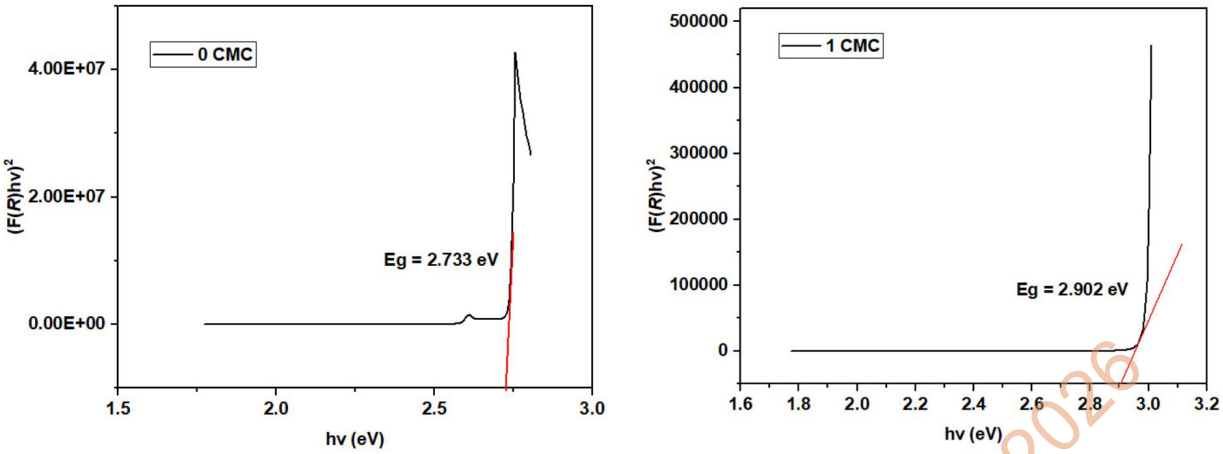

Figure 6. Tauc plot of direct TiO_2/ZnO/CuO 0 and 1 CMC composites

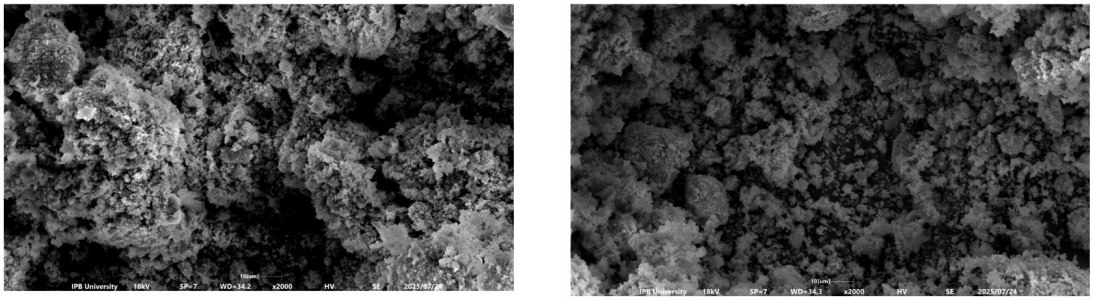

a) b)

Figure 7. SEM micrograph of TiO_2/ZnO/CuO composites, a) 0 CMC and b) 1 CMC

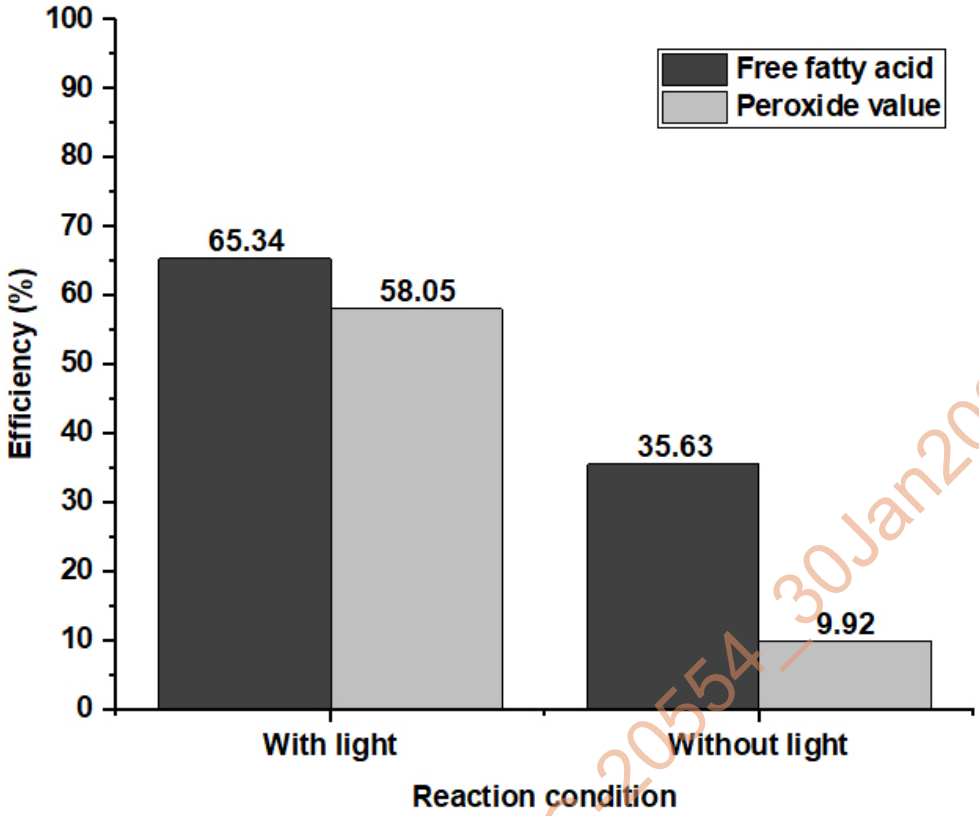

Figure 8. Photocatalyst performance under dark and light conditions

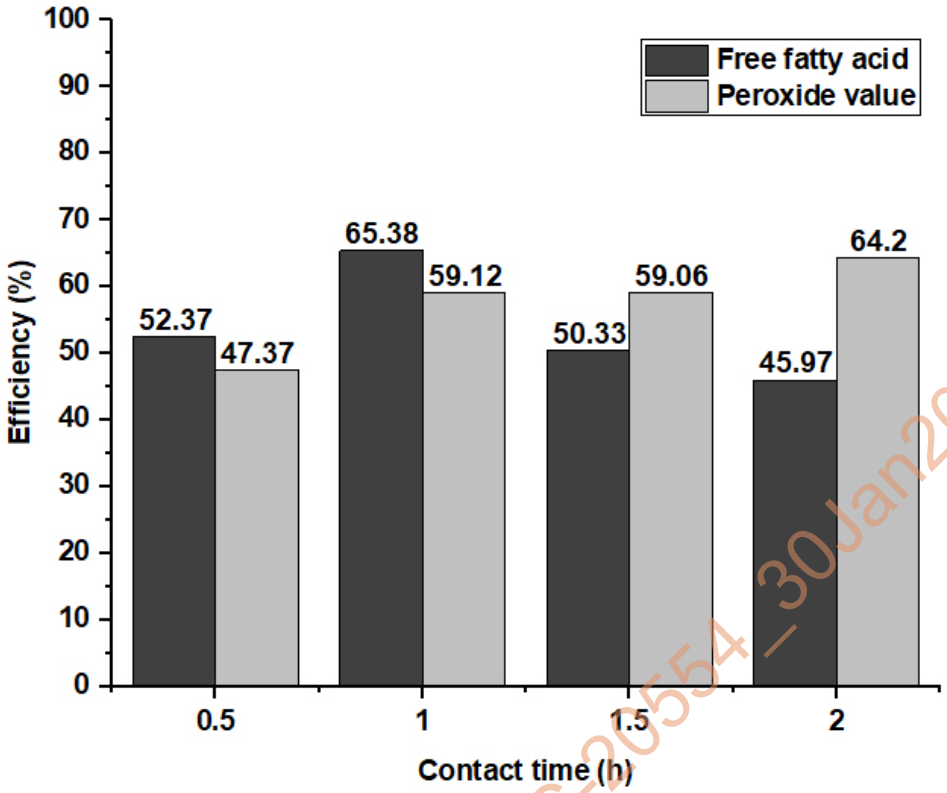

Figure 9. Optimization of the UCO photodegradation reaction time

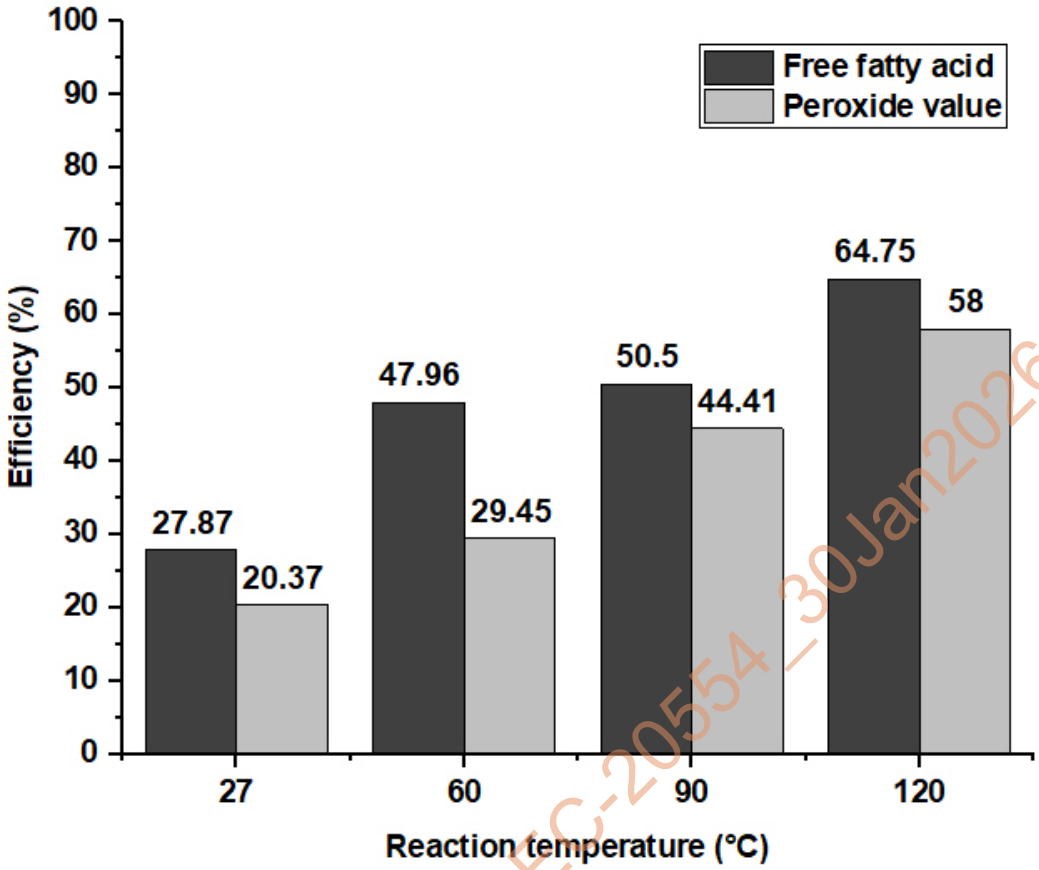

Figure 10. Optimization of the UCO photodegradation reaction temperature

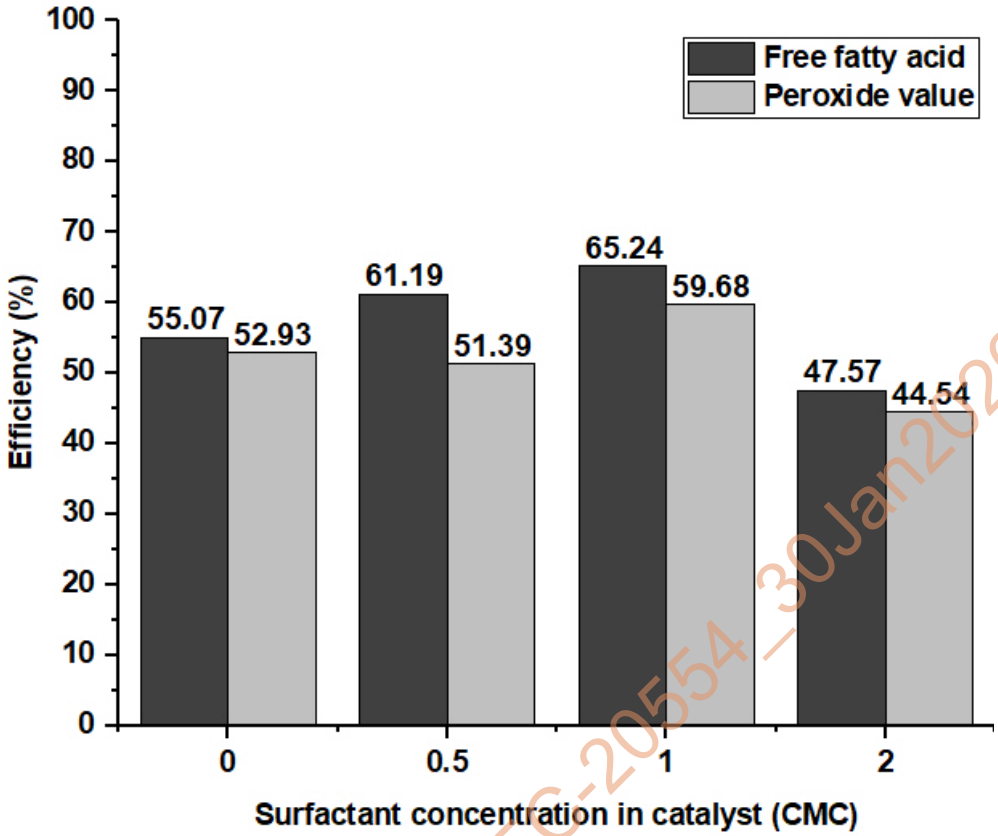

Figure 11. Optimization of surfactant concentration in catalyst UCO photodegradation

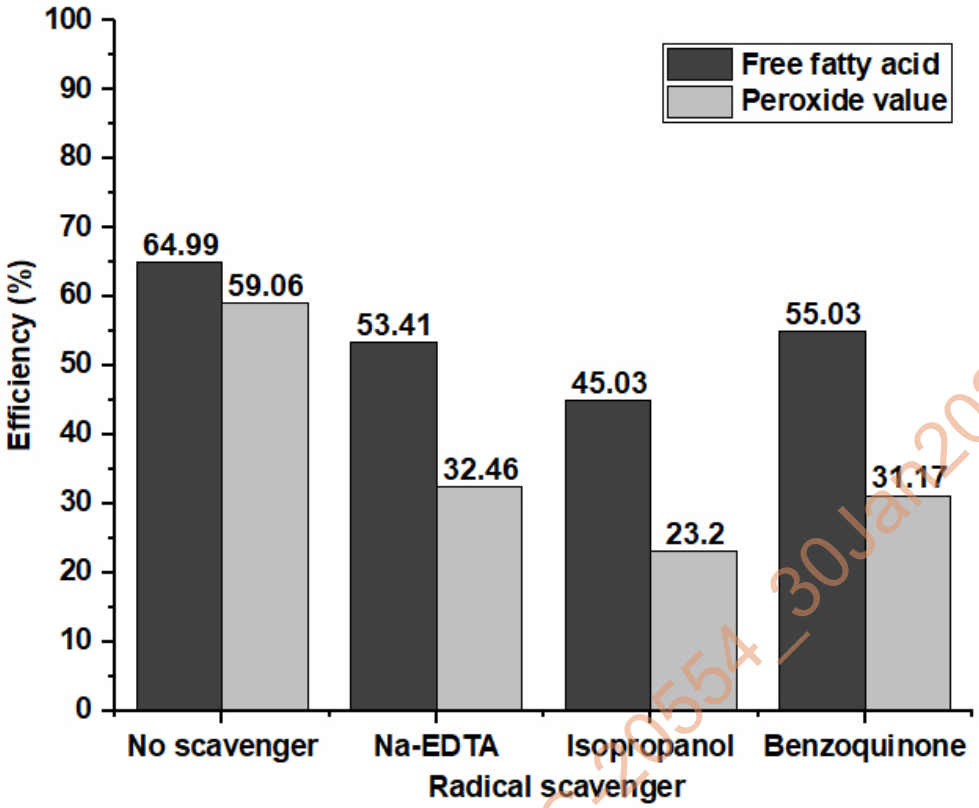

Figure 12. UCO photodegradation performance on various radical scavengers

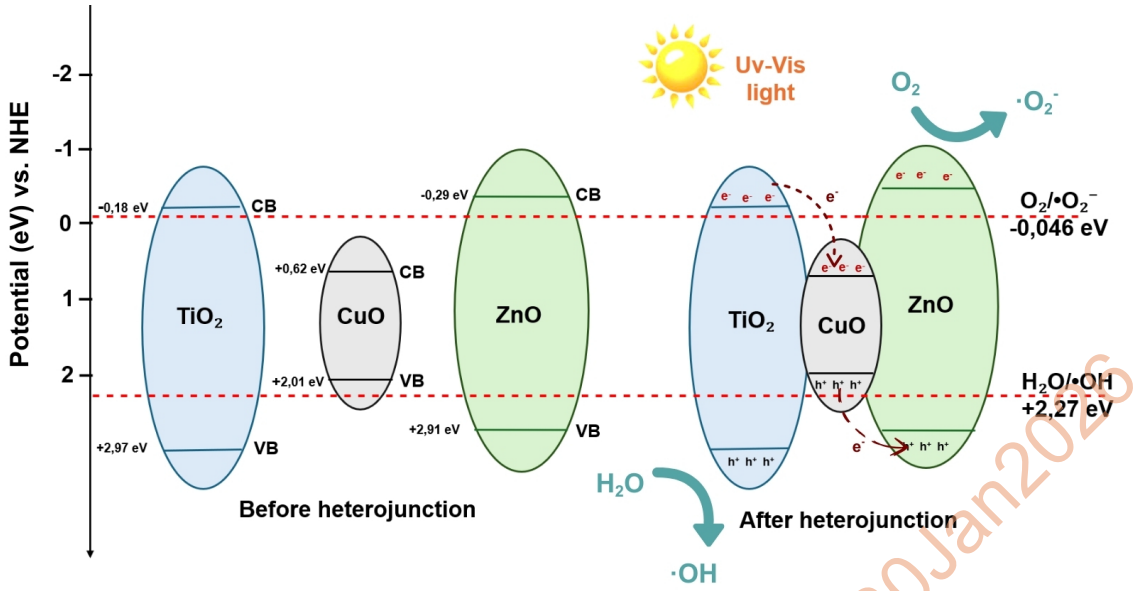

Figure 13. Potential mechanism of FFA and UCO peroxide with TiO_2/ZnO/CuO composite

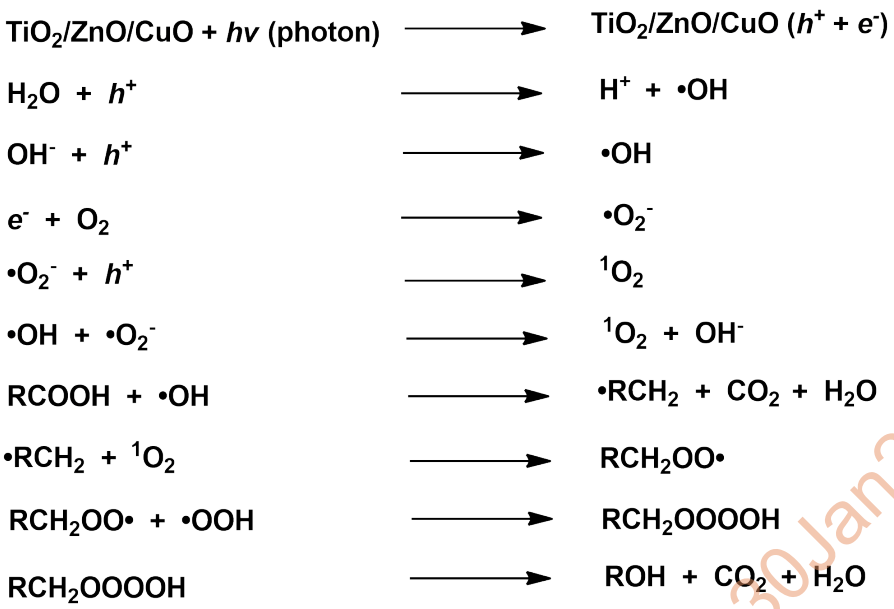

Figure 14. Mechanism of radical photodegradation of UCO

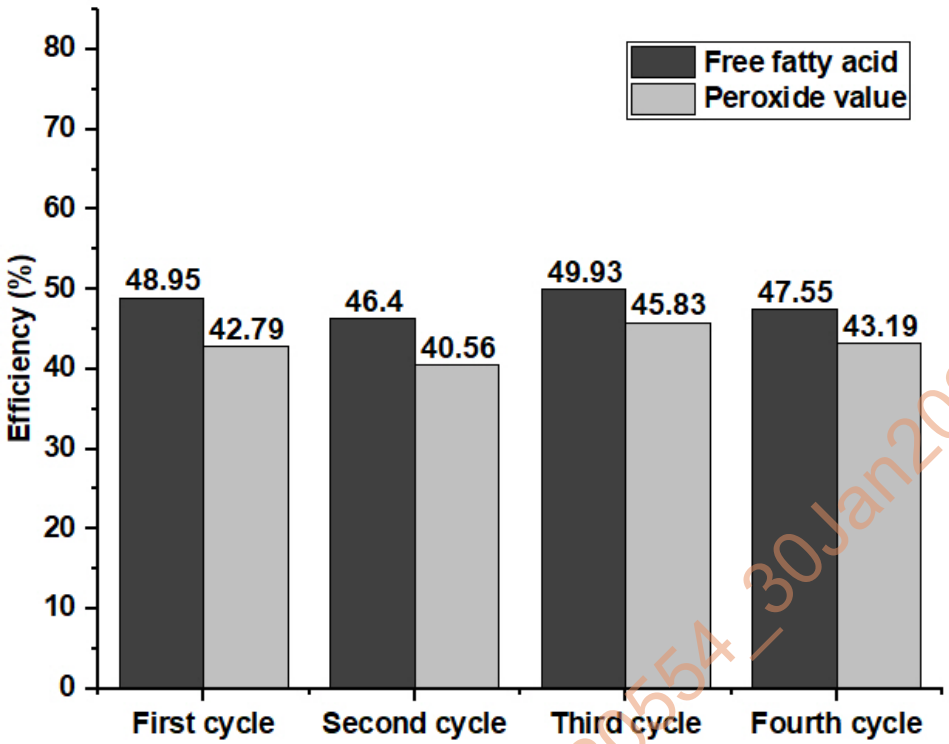

Figure 15. Photocatalytic performance of 2 CMC composites at various cycles

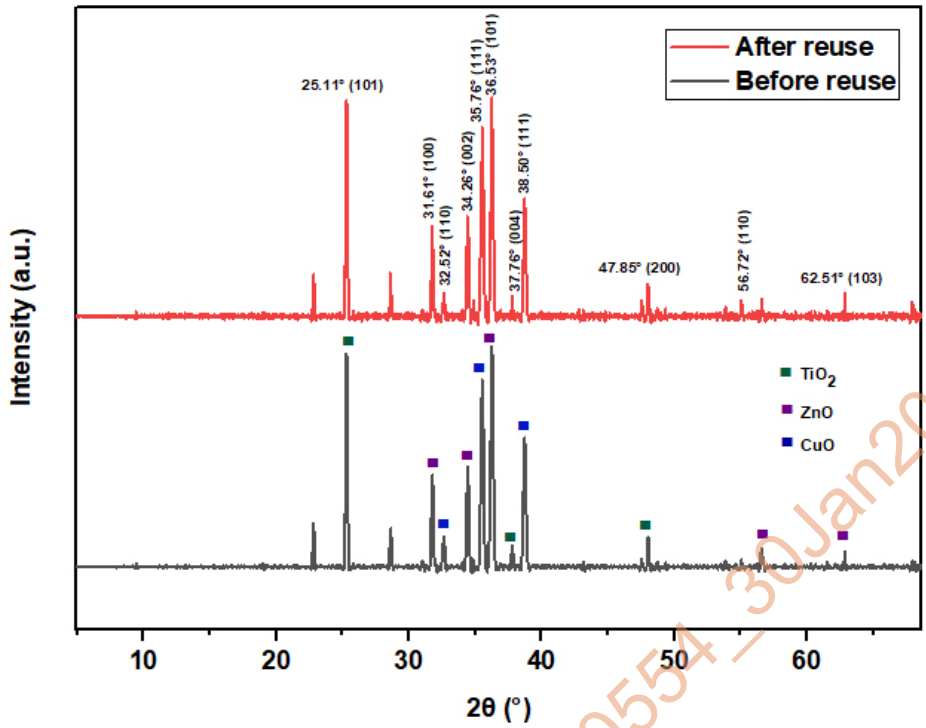

Figure 16. Comparison of XRD spectra of TiO_2/ZnO/CuO 2 CMC composites before and after reuse

Table 1. Characteristics of BET-BJH analysis results for TiO_2/ZnO/CuO 0 and 1 CMC composite

Composite TiO_2/ZnO/CuO	Surface area TiO_2/ZnO/CuO (m^2/g)	Average pore size TiO_2/ZnO/CuO (nm)	Total pore volume TiO_2/ZnO/CuO (cm^3/g)
0 CMC	17.421	4.37699	0.03812
1 CMC	43.377	3.87384	0.08402